Extended Abstracts of the 16th (1984 International) Conference on Solid State Devices and Materials, Kobe, 1984, pp. 115-119 **C-1-1**

**Invited**

# Monolithic Integration of GaAs and Si

John C. C. Fan

Lincoln Laboratory, Massachusetts Institute of Technology

Lexington, Massachusetts 02173-0073

This paper will review some of our recent developments in the monolithic integration of GaAs and Si (MGS). Such technology may eventually permit the fabrication of GaAs solar cells on inexpensive Si substrates, as well as the integration of Si and GaAs devices on the same wafer in order to take full advantage of the complementary capabilities of the two material systems. We will first discuss our results for GaAs solar cells on Si substrates. We will then briefly describe our initial results on GaAs MESFETs and AlGaAs diode lasers fabricated on MGS wafers.

## SOLAR CELLS

Attempts to grow GaAs on Si substrates by chemical vapor deposition (CVD) have been largely unsuccessful because of difficulties in nucleation (1). We have overcome these difficulties by coating Si substrates with a thin film of Ge before GaAs deposition (1). A similar approach using a Ge intermediate layer has also been reported by workers in Japan (2).

Initially we reported (1) the fabrication of small-area (0.6 mm diameter) shallow-homojunction $n^+/p/p^+$ GaAs solar cells with conversion efficiency of 14% (AM1, one sun) that were prepared on Ge-coated $p^+$ Si substrates. We recently reported (3) the successful fabrication of much larger cells of this type, a development made possible by improvements in both material preparation and cell fabrication procedures. The electrical and structural properties of the GaAs/Ge/Si cells have been studied in detail, and the effects of material defects on the solar cell characteristics are discussed. We have also previously reported (1) the fabrication of monolithic tandem cells composed of a shallow-homojunction GaAs top cell and a Si bottom cell that are connected by a thin Ge layer. We have now fabricated such cells in which a substantial increase in photocurrent has been achieved by etching stripe openings in the GaAs cell to expose corresponding regions of the Si cell directly to solar radiation. The results indicate that GaAs/Ge/Si structures could be used for the fabrication of single-junction cells on inexpensive Si sheets and also to provide substrates for the growth of AlGaAs or GaAsP for monolithic AlGaAs/Si or GaAsP/Si tandem cells.

### GaAs Single-Junction Cells

In making the GaAs/Ge/Si solar cells (see Fig. 1), the Si substrate was first coated with a Ge layer deposited by e-beam evaporation (3), and GaAs layers were then grown by CVD in an

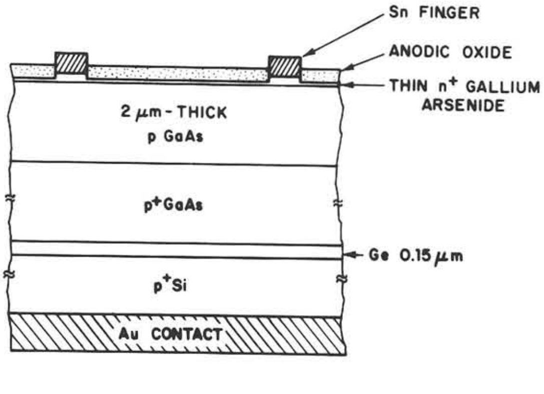


Fig. 1. Schematic diagram of a GaAs/Ge/Si solar cell.

$AsCl_3$-GaAs-$H_2$ system. The sample preparation and growth procedures were similar to those reported previously (1).

The techniques used for solar cell fabrication were similar to those used for GaAs cells on single-crystal GaAs substrates (4), which we shall refer to as conventional cells. Anodic oxide was used as an AR coating. The cell areas, which were defined by mesa etching, were ~0.093 or 0.51 $cm^2$. The cells have the following characteristics (3).

Figure 2 shows typical illuminated I-V curves for 0.093 and 0.51 $cm^2$ cells under simulated AM1, one-sun conditions. Both cells have an open-circuit voltage $V_{oc}$ of ~0.8 V and short-circuit current density $J_{sc}$ of ~23 $mA/cm^2$. The smaller cells have a better fill factor ff of ~0.75, giving an efficiency of ~14%. The efficiency of the larger cells is ~11%. Compared to the values for our conventional GaAs cells, $J_{sc}$ of the GaAs/Ge/Si cells is ~10% smaller, and $V_{oc}$ is ~20% smaller.

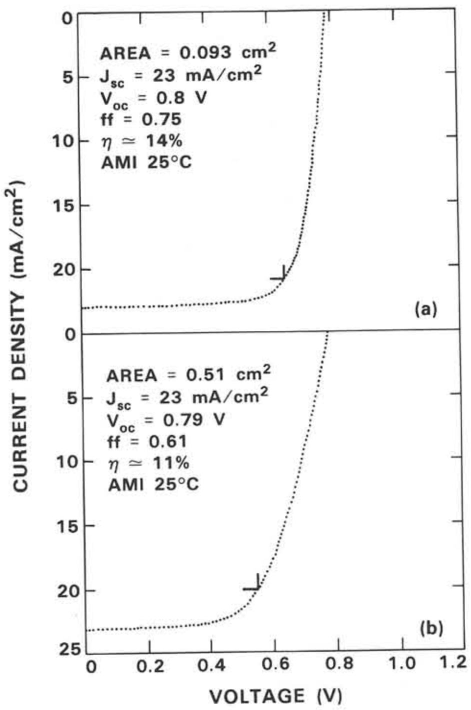


Fig. 2. I-V characteristics (AM1, one sun) of two GaAs cells on Ge-coated Si substrates.

The external quantum efficiency of the cell of Fig. 2(a) is plotted as a function of wavelength in Fig. 3. In comparison with values for conventional cells, the efficiency values in Fig. 3 are nearly the same at wavelengths up to 0.65 μm but 10-20% lower at the longer wavelengths. The relative decrease at the longer wavelengths indicates a lower minority carrier diffusion length in the base (p) region. Computer fitting of the quantum efficiency data

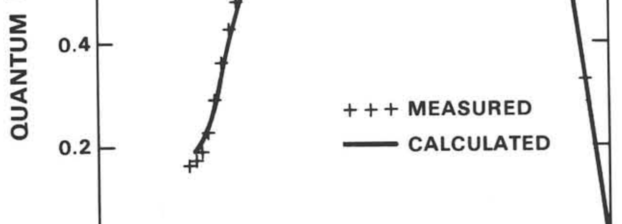


Fig. 3. External quantum efficiency as a function of wavelength for the cell of Fig. 2(a). The solid curve is calculated for a minority carrier diffusion length of 2 μm.

(solid curve in Fig. 3) yields a diffusion length of 2 μm, compared with 10-20 μm for conventional cells. Since the GaAs layers on Ge-coated Si contain ~$10^7$ cm$^{-2}$ dislocations (1), the reduction in the diffusion length is attributed to recombination at dislocations.

To investigate the diode properties of the solar cell n-p junction, the dependence of $J_{sc}$ on $V_{oc}$ was determined by measuring these quantities at illumination levels up to 15 suns. The result for the cell of Fig. 2(a) is shown in Fig. 4. From the relationship $V_{oc} = A\,(kT/q)\,\ell n[(J_{sc}/J_o) + 1]$, the diode factor

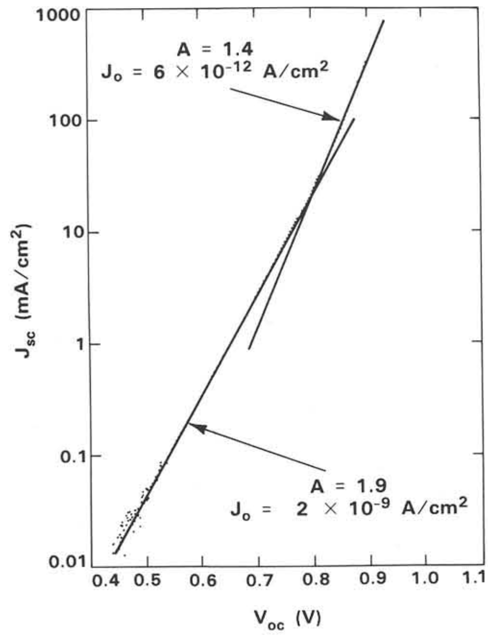


Fig. 4. Short-circuit current density $J_{sc}$ as a function of open-circuit voltage $V_{oc}$ at different illumination levels for the cell of Fig. 2(a).

A is 1.9 and the saturation (dark) current density $J_o$ is 2 x $10^{-9}$ A/cm$^2$ for $V_{oc}$ less than 0.8 V (illumination level less than one sun). For $V_{oc}$ larger than 0.8 V (multiple-sun illumination), the corresponding values are 1.4 and 6 x $10^{-12}$ A/cm$^2$.

The diode factor of almost 2 for low $V_{oc}$ indicates that the dark current is predominantly space-charge recombination current (5) due to the presence of dislocations near the junction region, rather than injection current, as in an ideal junction (3). From the relationship $J_o \simeq qn_iW/2\tau$, where $n_i$ is the intrinsic carrier concentration (1.8 x $10^6$ cm$^{-3}$) and W is the space-charge layer width (~2.5 x $10^{-5}$ cm), the minority carrier lifetime $\tau$ is estimated to be ~1.8 ns for $J_o$ = 2 x $10^{-9}$ A/cm$^2$. The diffusion length L (= $\sqrt{D\tau}$, where D is the diffusivity) is then ~3 μm, in reasonable agreement with the value obtained from the quantum efficiency data. The large diode factor also results in a degradation of the fill factor. The fill factor calculated (5) for a cell with $V_{oc}$ = 0.8 V and A = 2 is equal to 0.75, in agreement with our measured value for one-sun illumination. For high $V_{oc}$ (multiple-sun illumination), the diode factor and saturation current density improve, indicating that both injection current and recombination current contribute to the diode forward current.

GaAs-Si Monolithic Tandem Cells

We have also fabricated tandem cells composed of a GaAs top cell and a Si bottom cell. These devices use a monolithic structure formed by growing a GaAs shallow homojunction on a Ge layer 0.1 μm thick that is deposited on a lightly doped (0.1-1 Ω cm) p Si substrate. As a result of As diffusion through the Ge layer during GaAs growth, an n-p junction is formed in the Si substrate close to the Ge-Si interface. Several 0.093 $cm^2$ cells have been fabricated with $V_{oc}$ of 1.1-1.2 V and $J_{sc}$ of ~7 $mA/cm^2$. Figure 5(a) shows the I-V characteristics of a typical cell. The current density is relatively low because it is limited by the photocurrent generated in the Si cell.

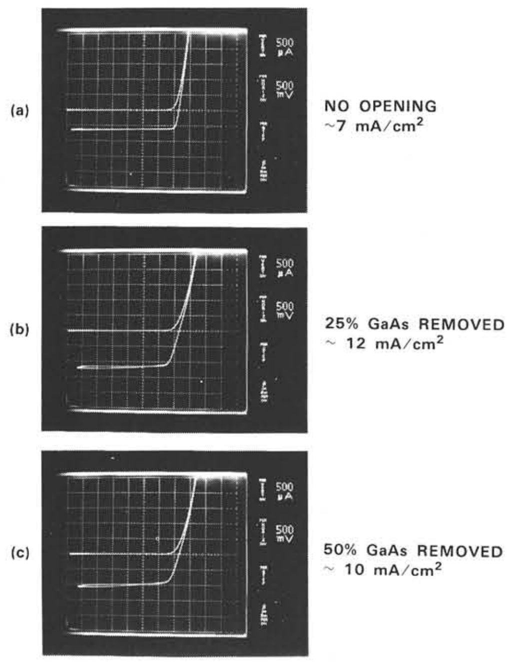


Fig. 5. I-V characteristics of GaAs-Si tandem cells for which (a) none, (b) 25%, and (c) 50% of the GaAs area was removed by etching.

To increase the photocurrent, in some tandem devices stripe openings were etched in the GaAs cell to expose the corresponding regions of the Si cell to direct solar radiation, as shown schematically in Fig. 6. When ~25% of the GaAs area was removed, $J_{sc}$ rose to ~12 $mA/cm^2$ [Fig. 5(b)], an increase of ~70%. The $V_{oc}$ remained nearly the same, but the fill factor decreased somewhat because the sheet resistance of the As-diffused $n^+$ layer in Si is quite high due to the extremely shallow junction. For this device the current density in the GaAs cell is now ~12/0.75 = ~16 $mA/cm^2$, smaller than the $J_{sc}$ of 23 $mA/cm^2$ observed for the single-junction GaAs/Ge/Si cells, indicating that the current is still limited by the Si cell. When 50% of the GaAs area was removed, $J_{sc}$ decreased to ~10

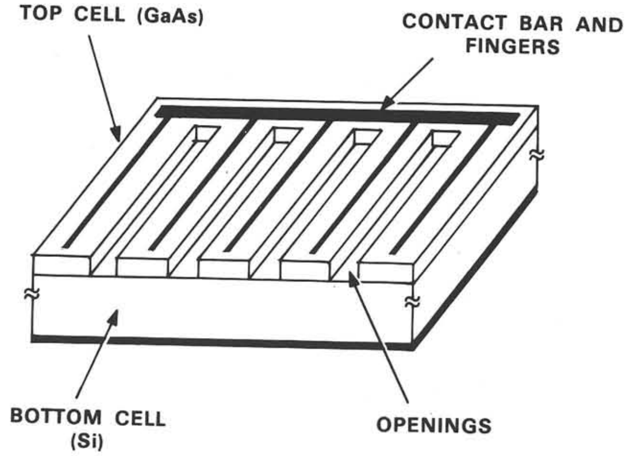


Fig. 6. Schematic diagram showing a GaAs-Si tandem cell with openings etched in the GaAs layers.

$mA/cm^2$ [Fig. 5(c)]. The current of this device is limited by the GaAs cell. The best result should therefore be obtained when the portion of the GaAs area removed is between 25 and 50%, consistent with the calculated optimum value (6) of ~30%. Use of this unequal-area design, in which the area of the top cell is less than that of the bottom cell, would enhance the potential usefulness of GaAs-Si tandem cells and in general permit a broader choice of materials for the component cells in series-connected tandem structures.

In summary, we have fabricated single-junction GaAs/Ge/Si solar cells with conversion efficiencies of 14 and 11% for areas of ~0.093 and 0.51 $cm^2$, respectively. Improvement in cell performance could be achieved by reducing overall dislocation density and by preventing dislocations from bending over parallel to the junction. We have also fabricated monolithic GaAs-Si tandem cells.

## GaAs MESFETs

Recently, we have succeeded in fabricating reasonably good GaAs MESFETs on GaAs layers grown on Ge-coated Si substrates (7). An undoped Ge layer is first deposited on a $p^+$-Si substrate. Three GaAs layers -- an undoped buffer layer, an n active channel layer and an $n^+$ contacting layer are then grown on the Ge layer. The GaAs layers have mirror smooth surfaces. The source and drain contacts are formed by Ge/Au/Ni. The gate region is recessed by etching, and the gate contact is made with Ti/Au. Figure 7 is an optical micrograph of a finished device.

Figure 8 shows the Schottky diode characteristic between the source and gate (2.1 μm long, 200 μm wide) of an MGS GaAs MESFET. From the data for the forward direction, the built-in voltage is about 0.67 V and the ideality factor is about 1.38. The reverse leakage current, which increases from about 3 μA at $V_{gs}$ = -1 V to about 12 μA at $V_{gs}$ = -2 V, is believed to be due to a high density of defects that propagate from the Ge/Si interface.

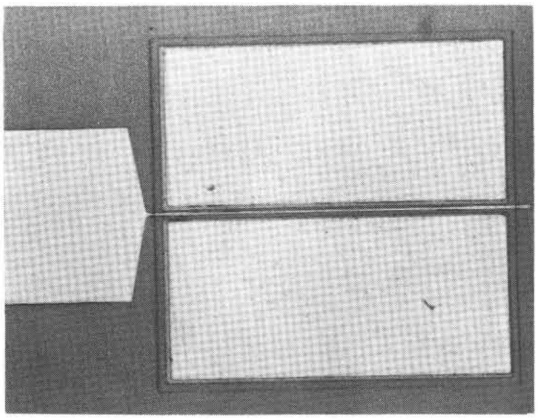

Fig. 7. Optical micrograph of MGS GaAs MESFET with gate length of 2.1 μm and gate width of 200 μm.

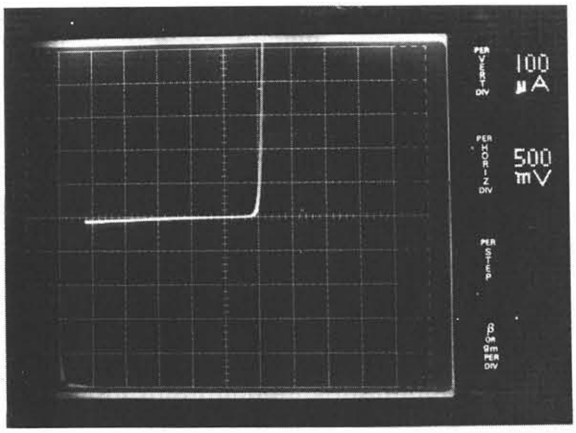


Fig. 8. Schottky diode characteristic between the source and gate of MGS GaAs MESFET.

Figure 9 shows transistor characteristics for another MGS GaAs MESFET with gate length of 2.1 μm and gate width of 200 μm. The top curve was obtained for $V_{gs}$ = 0.5 V. The transconductance measured at $V_{gs}$ = 0 V is about 105 mS/mm, which is comparable to the values obtained for MESFETs on GaAs substrates (8). This result suggests that the defect density in the GaAs active channel is not high enough to produce a marked reduction in the majority carrier mobility. However, the drain current is not completely turned off. A more detailed measurement at $V_{ds}$ = 2 V shows that the drain current reaches a minimum and then increases as $V_{gs}$ is made increasingly negative.

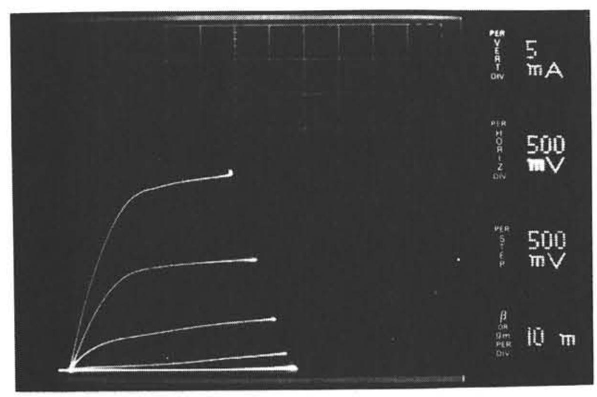


Fig. 9. Transistor characteristics of MGS GaAs MESFET. The top curve was obtained for $V_{gs}$ = +0.5 V.

## AlGaAs DOUBLE-HETEROSTRUCTURE DIODE LASERS

Recently, we have succeeded in fabricating the first AlGaAs double-heterostructure diode lasers grown on Si substrates (9). As in the case of MGS MESFETs, a thin Ge film was deposited by e-beam evaporation on a $p^+$ Si substrate before growth of the device structure.

Several devices randomly chosen from a single wafer were evaluated at room temperature by applying bias pulses of 50-100 ns at repetition rates of $10^2$-$10^3$ Hz. The spontaneous emission was very weak, and all the devices failed during attempts to increase the bias sufficiently to obtain stimulated emission. Ten more devices from the same wafer were then evaluated at ~77 K by applying 100-ns pulses at a 1-kHz repetition rate. One of the devices emitted superradiantly, but failed without lasing when the bias was increased to ~1 A. The remaining devices produced stimulated emission at values of threshold current ($I_{th}$) between 260 and 350 mA, except for one with a threshold of 700 mA. If current spreading under the stripe contact is neglected, the lowest threshold of 260 mA corresponds to a threshold current density of 10.8 kA/cm$^2$. For the device with this threshold the power output from one facet is plotted against current in Fig. 10.

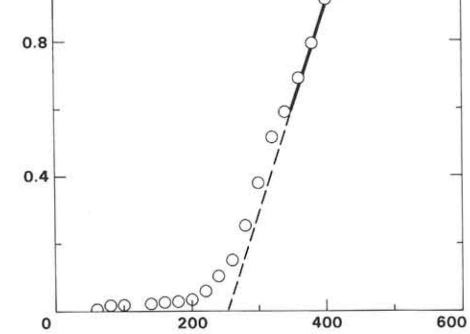


Fig. 10. Power emitted from one facet of an MGS AlGaAs diode laser as a function of pulsed bias current at 77K. The 0.7% quantum efficiency was calculated assuming equal power emission from both facets.

The differential quantum efficiency is 0.7%, assuming equal power emission from both facets. The maximum power output for the various devices ranged from ~1.6 to 1.8 mW per facet, corresponding to efficiencies from 0.6 to 1.2%. It is probable that the low values of output power and efficiency result largely from the high defect density in the grown layers. The measured etch pit density was ~5 x $10^6$ $cm^{-2}$.

The emission spectra were measured with a 0.5-m Czerny-Turner grating monochromator equipped with a photomultiplier incorporating a GaAs photocathode. Spectra obtained above and below $I_{th}$ for the lowest threshold laser, operating at ~77 K, are shown in Fig. 11. The

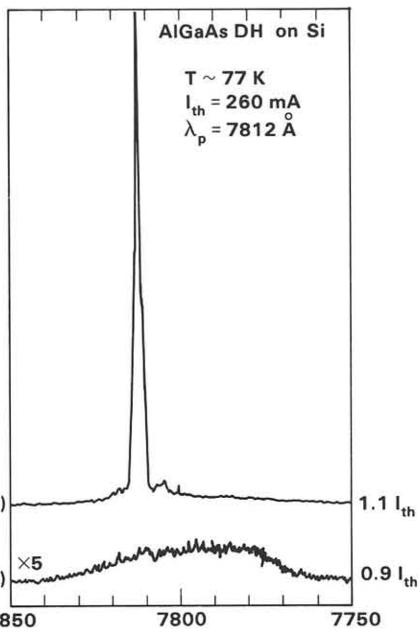


Fig. 11. Spectral emission from the lowest threshold laser exhibiting (a) nearly single mode oscillation at 1.1 $I_{th}$, and (b) spontaneous emission at 0.9 $I_{th}$.

emission at 1.1 $I_{th}$ is nearly single mode with maximum intensity at 7812 Å (1.587 eV). The presence of a second, lower intensity mode is evidenced by the shoulder on the short wavelength side of the dominant peak. A device with a threshold of 290 mA also exhibited a nearly single mode emission spectrum, peaked at 7787 Å (1.592 eV). The remaining devices had multimode emission spectra with a dominant peak about 6 db larger in intensity than the next highest one. In all cases the dominant peak, which ranged in wavelength from 7787 to 7812 Å, occurred on the long wavelength side of the spontaneous emission curve. The separation between the minor peaks was ~3 Å, which is characteristic of multiple longitudinal mode oscillation.

## CONCLUSION

Monolithic integration of GaAs and Si should have important applications for solar cells, diode lasers and FETs. Initial demonstration of these devices has already been achieved. Further improvements are required in the material quality of GaAs layers before high-performance devices can be made.

## ACKNOWLEDGEMENTS

I would like to acknowledge the collaboration of many colleagues at Lincoln Laboratory. This work was sponsored by the Solar Energy Research Institute and the Department of the Air Force.

## REFERENCES

1. R. P. Gale, J. C. C. Fan, B-Y. Tsaur, G. W. Turner and F. M. Davis, IEEE Electron Dev. Lett. EDL-2, 169 (1981).

2. Y. Shinoda, T. Nishioka and Y. Ohmachi, Jpn. J. Appl. Phys. Lett. 22, L450 (1983).

3. B-Y. Tsaur, J. C. C. Fan, G. W. Turner, B. D. King, R. W. McClelland and G. M. Metze, to be published in Proceedings of the 17th IEEE Photovoltaic Specialists Conference, Kissimmee, Florida, May 1984.

4. G. W. Turner and M. K. Connors, J. Electrochem. Soc. 131, 1211 (1984).

5. H. J. Hovel, Solar Cells, Vol. 11, Semiconductors and Semimetals (Academic Press, New York, 1975).

6. J. C. C. Fan, B-Y. Tsaur and B. J. Palm in Conference Record of the 16th IEEE Photovoltaic Specialists Conference, San Diego (IEEE, New York, 1982), p. 692.

7. H. K. Choi, B-Y. Tsaur, G. M. Metze, G. W. Turner and J. C. C. Fan, to be published in IEEE Electron Dev. Lett.

8. H. Fukui, Bell Syst. Tech. J. 58, 771 (1979).

9. T. H. Windhorn, G. M. Metze, B-Y. Tsaur and J. C. C. Fan, to be published in Appl. Phys. Lett.